Belkacem Kada*, Abdullah Algarni, Mostefa Bourchak and Mahmoud N. Nahas

Damage assessment of random multiwalled carbon nanotube-reinforced polymer nanocomposites

DOI 10.1515/secm-2015-0460
Received November 6, 2015; accepted October 1, 2016; previously published online November 29, 2016

Abstract: The paper presents a numerical procedure to evaluate the mechanical properties and predict the damage initiation of random multiwalled carbon nanotube-reinforced polymer nanocomposites (MWCNT-RPNC). The Hashin-Shtrikman (H-S) random prediction model is used to compute the properties of the reinforced polymer matrix, whereas the Chamis model is used to compute the lamina properties and the Hashin progressive damage model within the ABAQUS environment is used as a finite element analysis (FEA) tool to predict the damage initiation in the reinforced composite material. Experimental testing is employed to validate the numerical results and to adjust the H-S prediction model for MWCNT-RPNC.

Keywords: acoustic emission; composite damage; finite element analysis; nanocomposite mechanical characterization; random multiwalled carbon nanotubes.

1 Introduction

The excellent physical and mechanical properties of nanofiller materials have been the incentive to use multiwalled carbon nanotubes (MWCNTs) to reinforce polymer composite materials to enhance their physical and mechanical properties. Their outstanding properties such as high strength with miniscule size and very low weight have encouraged the application of MWCNT-reinforced polymer nanocomposites (MWCNT-RPNC). Reinforced nanocomposite materials are suitable not only for a wide range of advanced applications (e.g. aerospace and biomedical) but also as a test bed for fundamental science [1–4]. CNTs, particularly MWCNTs, have shown outstanding mechanical, electrical, and thermal properties. Extremely high mechanical properties such as strength-to-weight ratio, tensile strength, Young's modulus, flexibility, and toughness make MWCNTs good candidates for the reinforcement of materials in the form of nanocomposites.

Many experimental investigations have concluded that the enhanced mechanical properties of polymer matrices can be obtained by reinforcing these matrices with CNTs. Chandrasekaran et al. [5] found that the addition of 0.5 wt.% MWCNTs to composites enhanced the interlaminar shear strength from 27 to 32.8 MPa (i.e. 21% improvement) compared to neat samples. A carbon fiber-reinforced epoxy incorporated with 0.2, 0.3, and 0.5 wt.% fluorine functionalized CNTs f-XD-CNT was tested under two cycling loadings (tension-tension and tension-compression loading) to measure its tensile strength, stiffness, and durability [6]. The tensile strength of 0.5 wt.% f-XD-CNT reinforced polymer samples increased by 18% and their stiffness increased by 24% compared to 0.5 wt.% neat polymer samples. In that study, it was also observed that the most significant improvements were in the tension-tension cyclic life of 0.3 wt.% CNT polymer-reinforced specimens for which the minimum durability, tensile strength, and life increased by 70%, 42%, and 30%, respectively, compared to neat laminates. The interfacial shear strength (IFSS) of the fiber/matrix could be improved by dispersing the CNTs in the fiber sizing formulation as reported by Godara et al. [7]. Their study focused on the effect of CNTs on the IFSS of glass fiber/epoxy composites when dispersed in the fiber sizing and matrix. By conducting single-fiber pull-out tests, it was found that the dispersion of CNTs in the fiber sizing was the most effective way to increase IFSS, whereas combining CNT in the fiber surface and matrix was the least effective.

In parallel to experimental tests, many important theoretical and numerical studies were carried out using advanced approaches and techniques. An interesting 3D micromechanical semicontinuum finite element model (FEM) was developed by Mortazavi et al. [8] for computing the Young's modulus of single-walled CNT (SWCNT)-reinforced

***Corresponding author: Belkacem Kada,** Department of Aeronautical Engineering, Faculty of Engineering, King Abdulaziz University, Jeddah 21589, Kingdom of Saudi Arabia, e-mail: bkada@kau.edu.sa
Abdullah Algarni and Mostefa Bourchak: Department of Aeronautical Engineering, Faculty of Engineering, King Abdulaziz University, Jeddah 21589, Kingdom of Saudi Arabia
Mahmoud N. Nahas: Mechanical Engineering Department, Faculty of Engineering, King Abdulaziz University, Jeddah 21589, Kingdom of Saudi Arabia

polymer composites. Using a representative volume element (RVE) with a cylindrical model, the nanotubes were simulated by discrete spring-based FEM, whereas the matrix was considered as a continuum medium. The model was run for a range of volume fractions and different mechanical performance of the interfacial region. Important results were drawn from these tests. First, the mechanical elastic performance of SWCNT-reinforced composites highly depends on the atomistic microstructure of the CNTs as well as the stiffness of the interfacial region. Second, the computational model with high stiffness values of the interface leads to predictions similar to those obtained using the rule of mixture (ROM) equation. Third, no substantial enhancement of the nanocomposite was obtained when the nanotubes were very softly bonded to the matrix. It is worth noting that the model has many practical advantages, as it includes the discrete nature of the nanotubes and simulates the interfacial regions via discrete nanoscale elements. Wang et al. [9] conducted another interesting finite element analysis (FEA) to assess the effect of fiber orientation on the Young's modulus of unidirectional fiber-reinforced composites. Their study found that the Young's modulus depends on the fiber orientation angles, and the shear modulus has a significant effect on Young's modulus. In the comparative study reported by Mortazavi et al. [8], three different modeling approaches were used to compute the elastic modulus of random two-phase composite materials. These approaches are the Mori-Tanaka method, FEM, and strong contrast with maximum volume concentration 3% model. By comparing the results of these three models, it was found that higher elastic properties and thermal conductivity of the composite could be obtained using platelet fillers.

Fracture and fatigue strength is one of the contentious issue in reinforced polymer matrix composite field as a high percentage of failure is due to fracture and fatigue reasons. It was found in the work of Grimmer and Dharan [10] through a series of experiments that the addition of a small volume of MWCNTs to the matrix of glass fiber composites slightly decreases the cyclic delamination crack propagation rates of the reinforced matrix and increases both critical and subcritical interlaminar fracture toughness. Wicks et al. [11] reported that the reinforcement of woven polymer matrix with aligned CNTs improves their mechanical properties. Using CNT-reinforced specimens with fuzzy fiber plies, mode I fracture tests were conducted under the ASTM D5528 standard. The tests showed that the interlaminar and intralaminar mechanical properties were enhanced due to the addition of CNTs where the initiation toughness was improved by more than 60%, steady-state toughness by 76%, and intralaminar initiation fracture of the specimen by 19%.

The effect of CNTs on the damage initiation and propagation in woven carbon fiber-epoxy matrix was investigated experimentally by Greef et al. [12] using acoustic emission measurement. The experiments showed that the addition of CNTs to the epoxy matrix slightly improved the strength by 3.1% and the strain-to-failure ratio by 4.6%. Bortz et al. [13] found that the mechanical properties and fracture characteristics of carbon fiber-reinforced composites could be enhanced by adding carbon nanofibers (CNF). Low-viscosity liquid epoxy system, helical-ribbon CNFs, and high-strength PAN-based carbon fiber (based on polyacrylonitrile) were used in their study. Multiple test types according to ASTM were conducted in their work, including double cantilever beam, tensile test, and fracture toughness. The results proved that the addition of 1 wt.% CNT improved the tensile modulus, ultimate tensile strength, and compressive strength by 5%, 8%, and 6%, respectively, whereas the flexural strength and flexural modulus improved by 10% and the mode I interlaminar fracture toughness improved by 35%. On the other side, short-beam strength was reduced by 4%. One can refer to references [14–20] for more details on detecting, locating, and quantifying damage in composite structures made of carbon fibers and CNTs.

In this paper, we propose a new numerical procedure for damage assessment in random MWCNT-RPNC. Using uniaxial static tensile test, the main objectives of this study are to (1) predict the mechanical properties of random MWCNT-RPNC, (2) understand the deformation mechanism and damage initiation of MWCNT-RPNC with random distribution of nanotubes, and (3) compare the outcomes of the proposed procedure to those of experimental testing. Different from the case of conventional composite materials, the proposed three-step method is based on the use of three different prediction models: (1) nanotube-reinforced matrix properties using the Hashin-Shtrikman (H-S) prediction model, (2) composite material using the Chamis model, and (3) damage initiation prediction using the Hashin model within the ABAQUS environment.

2 Mechanical properties and damage assessment of random nanocomposite materials

2.1 H-S model

The H-S prediction model is a macroscopic model that assumes isotropic and quasi-homogenous composite,

where the dimensions and the shape of the nanotubes have no effects. The elastic moduli of the nanotube-reinforced matrix are computed using the upper and lower limits of bulk K and shear G moduli and the nanotube fiber volume fraction ϕ_f as follows [21]:

$$E_{u,l} = \frac{\alpha K_{u,l}}{1 + 3 * \mathrm{K}_{u,l} / G_{u,l}} \tag{1}$$

with

$$K_u = K_f + (1-\phi_f)\left[\frac{1}{K_m - K_f} + \frac{3\phi_f}{3K_f + 4G_f}\right]^{-1} \tag{2}$$

$$K_l = K_m + \phi_f\left[\frac{1}{K_f - K_m} + \frac{3(1-\phi_f)}{3K_m + 4G_m}\right]^{-1} \tag{3}$$

$$G_u = G_f + (1-\phi_f)\left[\frac{1}{G_m - G_f} + \frac{6\phi_f(K_f + 2G_f)}{5G_f(3K_f + 4G_f)}\right]^{-1} \tag{4}$$

$$G_l = G_m + \phi_f\left[\frac{1}{G_f - G_m} + \frac{6(1-\phi_f)(K_m + 2G_m)}{5G_m(3K_m + 4G_m)}\right]^{-1} \tag{5}$$

where subscripts u and l denote the upper and lower bounds, respectively. The bulk moduli of the matrix and the nanotube fiber, K_m and K_f, are given as

$$K_{m,f} = \frac{E_{m,f}}{3(1-2\nu_{m,f})} \tag{6}$$

$E_{m,f}$ and $\nu_{m,f}$ are the elasticity modulus and Poisson's ratio of the matrix m and nanotube fibers f, respectively. We introduced the parameter α in Eq. (1) as a tuning parameter to adjust the formulation according to the experimentation records. The value of α in the original H-S model is 9.

2.2 Chamis model

The Chamis model is considered as the trusted micromechanical model for elastic property evaluation compared to the ROM [22]. The model formulation is as follows:

$$E_{11} = V_f E_{11,f} + V_m E_m \tag{7}$$

$$E_{22} = \frac{E_m}{1 - \sqrt{V_f}\left(1 - \frac{E_m}{E_{22,f}}\right)} \tag{8}$$

$$\nu_{12} = V_f \nu_{12,f} + V_m \nu_m \tag{9}$$

$$G_{12} = \frac{G_m}{1 - \sqrt{V_f}\left(1 - \frac{G_m}{G_{12,f}}\right)} \tag{10}$$

$$G_{23} = \frac{G_m}{1 - \sqrt{V_f}\left(1 - \frac{G_m}{G_{23,f}}\right)} \tag{11}$$

with E_{11} and ν_{12} calculated using the ROM. The 1, 2, and 3 indicate the fiber direction and the two transverse directions to the fiber direction.

2.3 Hashin damage model

Here, we briefly describe the Hashin damage model with damage and failure criteria [23]. The Hashin model was developed under certain assumptions such as the behavior of undamaged material being linearly elastic, the behavior of fiber-reinforced plies being transversely isotropic, and the fiber axis being the transverse isotropy axis. Without considering kinking and buckling failures, the Hashin model relates the failure indices to the fiber and matrix failures through the values of the six failure mode indices. When the value of one of the Hashin indices just exceeds 1.0 at any material point, the damage initiates from this point immediately and continues to accumulate until the material loses its load-carrying capacity (critical damage value). In 3D formulation, Hashin failure indices F_k (k= 1, …, 6) are defined as stress functions through the following formulation:

Fiber tensile and compression failures:

$$\begin{cases} F_1 = f_f^T = \left(\dfrac{\hat{\sigma}_{11}}{X^T}\right)^2 + \left(\dfrac{\hat{\sigma}_{12} + \hat{\sigma}_{13}}{S_{12}^2}\right)^2 \text{ if } \hat{\sigma}_{11} \geq 1 \\ F_2 = f_f^C = \left(\dfrac{\hat{\sigma}_{11}}{X^C}\right)^2 \text{ if } \hat{\sigma}_{11} \geq 1 \end{cases} \tag{12}$$

Matrix tensile and compression failures:

$$\begin{cases} F_3 = f_m^T = \left(\dfrac{\hat{\sigma}_{22} + \hat{\sigma}_{33}}{Y^T}\right)^2 + \dfrac{\hat{\sigma}_{23}^2 - \hat{\sigma}_{22}\hat{\sigma}_{33}}{S_{23}^2} + \dfrac{\hat{\sigma}_{12}^2 + \hat{\sigma}_{13}^2}{S_{12}^2} \ \textit{if } \hat{\sigma}_{22} + \hat{\sigma}_{33} \geq 1 \\ F_4 = f_m^C = \left[\left(\dfrac{Y^C}{2S_{23}}\right)^2 - 1\right]\left(\dfrac{\hat{\sigma}_{22} + \hat{\sigma}_{33}}{Y^C}\right) + \left(\dfrac{\hat{\sigma}_{22} + \hat{\sigma}_{33}}{2S_{23}}\right)^2 \\ \qquad + \dfrac{\hat{\sigma}_{23}^2 - \hat{\sigma}_{22}\hat{\sigma}_{33}}{S_{23}^2} + \dfrac{\hat{\sigma}_{12}^2 + \hat{\sigma}_{13}^2}{S_{12}^2} \ \textit{if } \hat{\sigma}_{22} + \hat{\sigma}_{33} < 1 \end{cases} \tag{13}$$

Interlaminar tensile and compression failures:

$$\begin{cases} F_5 = f_l^T = \left(\dfrac{\hat{\sigma}_{33}}{Z^T}\right)^2 & \text{if } \hat{\sigma}_{33} \geq 1 \\ F_6 = f_l^C = \left(\dfrac{\hat{\sigma}_{33}}{Z^C}\right)^2 & \text{if } \hat{\sigma}_{33} < 1 \end{cases} \tag{14}$$

where $\hat{\sigma}_{ij}(i,j=1,2,3)$ are the components of the effective stress tensor with respect to the ply axes; S_{ij} (i, j=1, 2, 3; $i \neq j$) denotes the allowable shear strength components with respect to the material axis; X, Y, and Z denote the allowable tensile strength components with respect to the material directions; the superscripts T and C denote the tension and compression, respectively. The effective stress tensor $\hat{\sigma}$ is given by the following linear model:

$$\hat{\sigma} = M\sigma \tag{15}$$

Where σ is the true stress tensor and M is the damage operator

$$M = \begin{bmatrix} \dfrac{1}{(1-d_f)} & 0 & 0 \\ 0 & \dfrac{1}{(1-d_m)} & 0 \\ 0 & 0 & \dfrac{1}{(1-d_s)} \end{bmatrix} \tag{16}$$

d_f, d_m, and d_s are the damage variables for the fiber, matrix, and shear, respectively. These variables are derived from the damage variables related to the damage modes:

$$d_f = \begin{Bmatrix} d_f^t & \text{if } \hat{\sigma}_{11} \geq 0 \\ d_f^c & \text{if } \hat{\sigma}_{11} < 0 \end{Bmatrix} \tag{17}$$

$$d_m = \begin{Bmatrix} d_m^t & \text{if } \hat{\sigma}_{22} \geq 0 \\ d_m^c & \text{if } \hat{\sigma}_{22} < 0 \end{Bmatrix} \tag{18}$$

$$d_s = 1-(1-d_f^t)(1-d_f^c)(1-d_m^t)(1-d_m^c) \tag{19}$$

The Hashin damage model is integrated in the ABAQUS environment through the following multistep procedure.

Step 1: Evaluation of damage initiation index F_k.

Step 2: Computation of equivalent displacement δ_{eq} and stress σ_{eq}.

Step 3: Computation and storage of equivalent displacement δ_{eq}^0 and stress σ_{eq}^0 at the onset to damage.

Step 4: Computation of equivalent displacement δ_{eq}^f at full damage.

Step 5: Updating the damage variables

$$d_k = max\left[d_{k,old},\ \delta_{eq}^f\left(\delta_{eq}-\delta_{eq}^0\right)/\delta_{eq}\left(\delta_{eq}^f-\delta_{eq}^0\right)\right] \tag{20}$$

We refer here to the work by Lapczyk and Hurtado [24] for the computation of different displacements and stress.

3 Numerical and experimental assessment of damage in MWCNT-RPNC

3.1 Specimen configuration

Glass fiber-reinforced plastic nanocomposite (GFRPNC) laminates with 16 layers $[90_4,0_4]_s$ were chosen for this work to investigate matrix cracking in mainly the 90° plies of the standard cross-ply laminates. The latter is known to suffer matrix cracking while under tensile load. The laminates were made using three components: glass fiber (Interglas-92145), epoxy resin (EPOLAM 2063), and randomly dispersed MWCNTs (Cheap Tubes, Inc). The fraction volume of MWCNTs was 0.1 wt.% and their inner diameters, outer diameters, and length are 3 to 5 nm, 8 to 15 nm, and 10 to 50 μm, respectively. After a thorough literature review, it was concluded that the 0.1 wt.% ratio is the most effective; hence, it was chosen for this investigation that is not comparative in nature.

To prepare the samples, MWCNTs were dissolved in ethanol and then dispersed using a ultrasonication probe for 1 h. The resulting solution was dissolved in epoxy resin for 30 min at 80°C using a magnetic stirrer and then mixed again for 30 min using the ultrasonication probe. The hardener was then added and the solution was magnetically stirred for another 30 min. Finally, the obtained nanocomposite matrix system was used to make the GFRP laminates using the resin infusion technique. Specimens were then cut according to the ASTM standard D3039. The nominal dimensions of the specimens were $20 \times 100 \times 2.5$ mm, which were selected based on the standard size of the diamond saw of the cutting machine. The reinforced materials and resin mechanical properties are shown in Table 1.

3.2 Experimentation

The equipment used in this investigation consisted of MTS809 axial/torsional servohydraulic system for testing and Vallen AMSY-6 acoustic emission system for measurement as shown in Figure 1.

Table 1: Mechanical properties of the components and fillers of GFRPNC.

Property	Resin (EPOLAM 2063)	MWCNTs (Cheap Tubes, Inc.)	Glass fiber (Interglas-92145)
Young's modulus (E)	3.100 GPa	764 GPa	33.00 GPa
Shear modulus (G)	0.055 GPa	280 GPa	0.050 GPa
Poisson's ratio (ν)	0.35	0.32	0.20
Volume fraction (V)		0.10 (10%)	0.40 (40%)

Figure 1: Experimental equipment configuration.

Three static tests were conducted using tensile load. The tests were conducted at a displacement rate of 2 mm/min and the load-displacement data were automatically recorded by the measurement system.

3.3 Numerical simulations

A preliminary step to the FEM simulation is the calculation of the mechanical properties of the GFRPNC. First, the properties of the reinforced resin with MWCNTs were computed using the H-S model. Then, the composite material (resin, MWCNTs, and glass fiber) properties were calculated using either the ROM or the Chamis model. These calculations resulted in the five properties required for FEA and shown in Table 2.

Table 2: Mechanical properties of reinforced resin and GFRPNC.

Properties	Resin with MWCNT (original H-S model)	Resin, MWCNT, and glass fiber (ROM)	Resin, MWCNT, and glass fiber (Chamis model)
E_{11}	20.073 GPa	25.244 GPa	25.244 GPa
E_{22}	20.073 GPa	23.803 GPa	26.684 GPa
G_{12}	7.860 GPa	123.818 MPa	78.765 MPa
G_{23}	7.860 GPa	123.818 MPa	78.765 MPa
ν_{12}	0.35	0.29	0.29

A 3D simulated plate was developed using ABAQUS software to evaluate the mechanical properties and identify the damage initiation strain and stress levels in the GFRPNC. After many FEM simulations using different values of the parameter α in Eq. (1), we have found that for $\alpha = 45$ the H-S model provides good predictions according to the experimental tests. Figure 2 shows a comparison between FEM calculations and the values of the data recorded for the three specimens.

4 Results and discussion

Figure 2 shows the load-displacement curves obtained from both experimental testing and numerical analysis.

Acoustic emission monitoring revealed that the damage was occurring as early as 15% of ultimate tensile strength for all the specimens. This observation was achieved through the monitoring of acoustic emission energy during the tensile tests. Figure 3 shows the stress-strain test of specimen 1 and its corresponding signal strength energy-strain data.

The main results are summarized in the following points.

1. By plotting the stress-strain curves, an average ultimate tensile strength of 418 MPa and ultimate tensile strain of 0.032 were recorded.

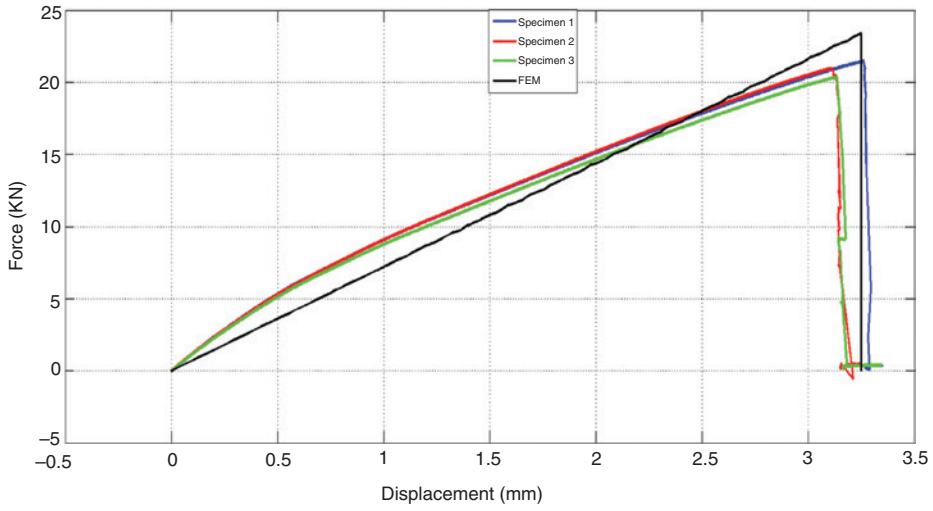

Figure 2: Load-displacement curves associated with FEM simulation and tensile tests.

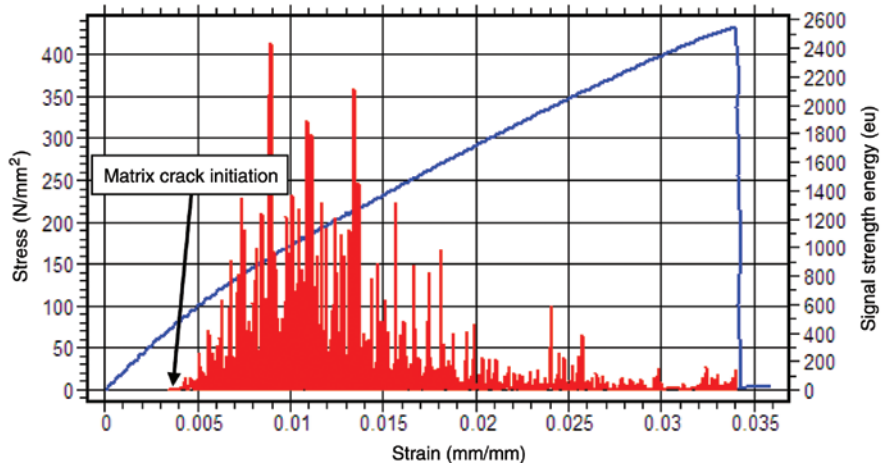

Figure 3: Stress-strain curve superimposed with acoustic emission energy data for specimen 1.

2. Microcracking initiates early in MWCNT-GFRPNC.
3. The H-S model for random nanocomposite-reinforced resin needs an adjustment by tuning the parameter α.
4. The difference between FEM simulation and experimentation findings is due to the material faults, bond conditions, and other similar factors, which are not easy to include in the numerical models used for simulation.

5 Conclusion

Damage initiation of random reinforced nanocomposite materials was investigated in this study using experimentation and FEM simulations. Experimental results indicate that microcracking initiates early at low loading conditions in MWCNT-GFRPNC materials. Numerical simulations indicate that the H-S model used for computing the mechanical properties of randomly reinforced resin has to be adjusted according to the experimentation tests. The H-S model output might be affected by many factors such as the distribution of the nanotubes in the resin, the bond conditions between nanotubes and resin, and the topology of the nanotubes themselves. Future works will focus on these issues and other factors such as fiber orientations, nanotube volume ratio, and dynamic tests.

Acknowledgments: This project was funded by the Deanship of Scientific Research (DSR), King Abdulaziz University, Jeddah, under grant no. 202/135/1431. The authors thank the DSR for the technical and financial support.

References

[1] Coleman JN, Umar K, Werner JB, Gun'ko YK. *Carbon* 2006, 44, 1624–1652.
[2] Mora RJ, Vilatela JJ, Windle AH. *Compos. Sci. Technol.* 2009, 69, 1558–1563.
[3] Mirjalili V, Hubert P. *Compos. Sci. Technol.* 2010, 70, 1537–1543.
[4] Corcione CE, Frigione M. *Materials* 2012, 5, 2960–2980.
[5] Chandrasekaran VCS, Advani SG, Santare MH. *Carbon* 2010, 8, 3692–3699.
[6] Davis DC, Wilkerson JW, Zhu J, Ayewah DOO. *Compos. Struct.* 2010, 92, 2653–2662.
[7] Godara A, Gorbatikh L, Kalinka G, Warrier A, Rochez O, Mezzo L, Luizi F, Vuure AW, Lomov SV, Verpoest I. *Compos. Sci. Technol.* 2010, 70, 1346–1352.
[8] Mortazavi B, Baniassadi M, Bardon J, Ahzi S. *Compos. Pt. B* 2013, 45, 1117–1125.
[9] Wang HW, Zhou HW, Gui LL, Ji HW, Zhang XC. *Compos. Pt. B* 2014, 56, 733–739.
[10] Grimmer CS, Dharan CKH. *Compos. Sci. Technol.* 2010, 70, 901–908.
[11] Wicks SS, Villoria RG, Wardle BL. *Compos. Sci. Technol.* 2010, 70, 20–28.
[12] Greef ND, Gorbatikh L, Godara A, Mezzo L, Lomov SV, Verpoest I. *Carbon* 2011, 49, 4650–4664.
[13] Bortz RD, Merino C, Martin-Gullon I. *Compos. Sci. Technol.* 2011, 71, 31–38.
[14] Gao L, Chou TW, Thostenson ET, Zhang Z, Coulaud M. *J. Carbon* 2011, 49, 3382–3385.
[15] Pandey G, Wolters M, Thostenson ET, Heider D. *J. Carbon* 2012, 50, 3816–3825.
[16] Wu AS, Coppola AM, Sinnott MJ, Chou TU, Thostenson ET. *J. Compos. Sci. Technol.* 2012, 72, 1618–1626.
[17] De-Villoria RG, Yamamoto N, Miravete A, Wardle BL. *J. Nanotechnol.* 2011, 22, 185502.
[18] Naghashpour A, Hoa SV. *J. Compos. Sci. Technol.* 2013, 78, 41–47.
[19] Naghashpour A, Hoa SV. *J. Nanotechnol.* 2013, 24, 455–502.
[20] Naghashpour A, Hoa SV. *J. Struct. Health Monitor.* 2015, 14, 35–45.
[21] Hu H, Onyebueke L, Abatan A. *J. Miner. Mater. Charact. Eng.* 2010, 9, 275–319.
[22] Younes R, Hallah A, Fardoun F, Chehade F. Comparative review study on elastic properties modeling for unidirectional composite materials. In *Composites and Their Properties,* Ning Hu N, Ed., INTECH Open Access Publisher: Rijeka, Croatia, 2012, 391–408.
[23] Hashin Z. *ASME J. Appl. Mech.* 1980, 47, 329–334.
[24] Lapczyk I, Hurtado JA. *Compos. Pt. A* 2007, 38, 2333–2341.